

# **Fabrication and Characterization of Giant Magnetoresistive (GMR) Sensor Microelectromechanical System (MEMS) Device**

**R. Ramesham\***, J. D. Olivas<sup>1</sup>, S. Stokes<sup>2</sup>, W. Wilson<sup>2</sup>, and Edward Generazio<sup>3</sup>

\*Jet Propulsion Laboratory, California Institute of Technology  
4800 Oak Grove Drive, Pasadena, CA 91109

<sup>1</sup>Lyndon B. Johnson Space Center, 2101 NASA Road 1, Houston, TX 77058

<sup>2</sup>Rice University, Houston, TX 77005

<sup>3</sup>Langley Research Center, Hampton, VA 23681-2199

## **ABSTRACT**

This paper discusses the fabrication aspects of a sensor device that is based on a sputter deposited multilayer giant magnetoresistive (GMR) sensor. The device consists of a micromachined microstructure (membrane), GMR sensor, and a sputtered hard magnetic thin film element onto microstructure. The GMR sensor device in principle detects acceleration by sensing changes in magnetic field caused by the displacement of the hard magnetic film on the microstructure. Very thin (0.5  $\mu\text{m}$ ) silicon nitride membranes are fabricated by means of anisotropic bulk micromachining of silicon wafer. Our objective in this study is to address the nature of spin valve structures (giant magnetoresistance in magnetic multilayers) and reliability issues in microelectronics fabrication of GMR sensor devices that exhibit the large magnetoresistive effect. A reliable GMR/MEMS device may have the characteristics such as a significant percentage change in resistance, high field resistance, low resistance noise, and a high bandwidth. These characteristics are very sensitive to the thickness of the various layers in sensor device multilayers, the composition and microstructure of the individual layers. Deposition and patterning of hard magnetic film over the microstructure and the bonding of microstructure over the GMR element have been attempted. The fabrication and reliability issues associated with GMR sensor devices have been discussed.

**KeyWords:** GMR, MEMS, spin valves, micromachining, and hard magnetic thin films.

## INTRODUCTION

The measurement of acceleration has been accomplished using several technologies in high-reliability applications such as guidance control, detonation, and shock/vibration measurement. Electromechanical, piezoelectric, piezoresistive, and capacitive acceleration sensors are available and the literature pertinent to giant magnetoresistive sensors for the above applications are scanty. All accelerometers require the conversion of acceleration into a force, causing a displacement, which is then turned into an electrical signal. This displacement is resisted by a calibrated spring of some kind.

$$\begin{array}{ll} F = ma & 1 \\ F = -kx & 2 \\ a = -kx/m & 3 \end{array}$$

Where  $F$  = force,  $m$  = Mass,  $a$  = Acceleration,  $k$  = spring constant, and  $x$  = displacement. Equations describing accelerometers are simple and well known. Accelerometers measure “ $a$ ” by knowing “ $k$ ” and “ $m$ ”, observing “ $x$ ” and using eqn. 3.

The giant magnetoresistive (GMR) effect was discovered in perfect-crystal samples exposed to very high magnetic fields.[1] The GMR effect was recently discovered in sputtered metallic thin films consisting of magnetic layers a few nanometers thick separated by equally thin nonmagnetic layers. Large decrease in the resistance of these films is observed when a magnetic field is applied. The cause of this effect is the spin dependence of electron scattering and the spin polarization of conduction electrons in ferromagnetic metals. With layers of the proper thickness, adjacent magnetic layer couple antiferromagnetically to each other with the magnetic moments of each magnetic layer aligned antiparallel to the adjacent magnetic layers. Frequent scattering of

electrons results in high electrical resistivity of the GMR device. If an external field overcomes the antiferromagnetic coupling it achieves parallel alignment of moments in adjacent ferromagnetic layers; the spin dependent scattering of conduction electrons is decreased and resistivity decreases. The size of this decrease in resistivity can be 10% to 20% and higher in GMR materials with multiple nonmagnetic layers.[2,3]

The significant advantage of GMR sensor materials is the greater sensitivity to applied magnetic fields. This increased sensitivity of the sensor materials makes it possible to detect smaller change in the magnetic fields. Large signals from GMR material structures also help overcome electronic noise. The difference between magnetoresistive (MR) and GMR sensors is sensitivity measured by percent change in resistance. In a MR sensor a resistance change is caused by the intrinsic property of the sensing layer. In a GMR sensor a resistance change is caused by the quantum nature of electrons such as electron spins. [2-4]

GMR sensors are composed of four thin films such as a sensing layer, a conducting spacer layer, a pinned layer, and an exchange layer. The thickness of all these layers is very thin (nanometers) except for the exchange layer which will allow the conduction of electrons to frequently move back and forth between the sensing and pinned layers via the conducting spacer layer. The magnetic orientation of the pinned layer is fixed and held in place by the adjacent exchange layer, while the magnetic orientation of the sensing layer changes in response to the external magnetic field. A change in the magnetic orientation of the sensing layer will cause a change in the resistance of the combined sensing and pinned layers. GMR sensor materials have two spin directions known as spin up and spin down. Conduction electrons with a spin direction parallel to a material's magnetic orientation move freely and therefore resulting in low electrical resistance. Conduction electrons with spin direction opposite to the materials magnetic

orientation are hindered by more frequent collisions with atoms in the material, which will result in higher electrical resistance.[4]

GMR sensors directly detect the magnetic field and they are sensitive to small changes in the magnetic fields, and can be used to measure position or displacement in linear and rotational systems. Some of the applications for GMR magnetic sensors are current sensing, linear or rotatory motion detection, linear or rotatory position sensing, ignition timing, throttle position sensing, etc.[3] GMR sensors have greater output than conventional anisotropic MR sensors.

The magnetic field  $H$  adjacent to hard magnetic thin film will hold the following relationship:

$$H = H_0 e^{-\alpha d/\lambda} \quad 4$$

Where  $\alpha$  is the constant of order,  $\lambda$  is the average distance between domains in the magnetic thin film and  $d$  is the distance between the GMR sensor and the hard magnetic thin film on the microstructure that certainly depends on the acceleration.

In this paper, we discuss the fabrication of GMR/MEMS sensor device that requires the deposition and characterization of GMR sensor materials, deposition and patterning of hard magnetic thin films over the microstructure, and microstructure fabrication using either surface micromachining and bulk micromachining of single crystal silicon substrate that are normally used in fabrication of MEMS devices.

## EXPERIMENTAL DETAILS

Direct current (DC) magnetron sputtering has been used to deposit thin film multilayers in a nanometer thickness range in an ultra high vacuum (UHV) chamber to fabricate GMR sensor element. The silicon dioxide has been grown over single crystal silicon substrate using thermal

oxidation, which was used as a substrate in this study to fabricate GMR sensor element. The sputtering of GMR element materials was performed at room temperature in argon ambient. The silicon dioxide/silicon substrate was mounted away from the target in the vacuum chamber. The structure of a typical spin valve is silicon/silicon dioxide/tantalum/copper/cobalt/FeMn/ Tantalum. Cobalt layer has been inserted between the permalloy and copper to enhance the GMR ratio and that will protect permalloy from mixing with the copper. Carbon and oxygen impurities in various layers have been observed to be reducing the GMR performance. Table 1 shows the typical deposition parameters employed to deposit GMR device stack layers by DC magnetron sputtering process in a UHV chamber. We have analyzed the multilayer GMR device structure with energy dispersive x-ray analysis (EDAX) to identify and confirm the elements present in as-deposited thin films. We have identified all the elements as anticipated with EDAX analysis except copper. The thickness of copper is less than a nanometer in the particular device structure tested. Figure 1 shows the EDAX analysis of the as-deposited stacked GMR element used to fabricate microsensor.

Thickness of the copper spacer layer, temperature stability, electrostatic discharge, change in magnetization, patterning of GMR element by lift-off process, annealing of hard magnetic thin film, and the field damage will influence the reliability of GMR characteristics.[5] The production of spin valves uses an IrPtMn antiferromagnetic layer as a pinning layer for the spin valves. This layer can withstand cycling temperature up to 350°C. Cobalt and copper do not mix at moderate temperatures, however permalloy and copper do mix and if permalloy is used adjacent to copper, the spin valve will degrade around 200°C. GMR layers are extremely thin, only about 300 – 400 Å (30 – 40 nm), so the temperature rise from a voltage spike can possibly melt the layers. There is also other possibility that of the magnetization changes if the temperature of the layer exceeds

the Neel temperature of the antiferromagnetic layer. The GMR sensor material should have resistance to electrostatic discharge and resistance to thermal degradation.

**Fabrication of GMR sensor:** The fabrication of GMR sensor involves three steps and they are as follows: 1. Fabrication of GMR sensor on the substrate, 2. Fabrication of the movable microstructure such as a membrane and finally, 3. Deposition of hard magnetic thin film onto the movable microstructure. Critical issues associated with the fabrication of a GMR sensor device are signal to noise ratio, geometry and lithographic definition of the spin valve on the substrate, magnetic properties of hard magnetic thin film, and process integration with surface and bulk micromachining processes.[6]

Figure 2 shows the schematic of the complete GMR/MEMS sensor device. A silicon substrate has been chosen in this study and silicon nitride was deposited using low-pressure chemical vapor deposition (LPCVD) process. Silicon nitride on one side of the silicon substrate was patterned and plasma etched down to the silicon substrate. The silicon substrate was anisotropically etched until silicon nitride onto the other side of the silicon substrate to fabricate very thin silicon nitride membranes. Another silicon substrate has been chosen and the growth of silicon dioxide was performed by thermal oxidation. Giant magnetoresistive element has been fabricated using lift-off technique onto the silicon dioxide. These two chips will be bonded using anodic bonding or any other appropriate technique to assemble the device as shown in the Fig. 2. [7]

The GMR element may be characterized by its change in resistance  $\Delta R/R$  when the field changes by an amount of  $\Delta H$ . The ratio of  $\Delta R/\Delta H$  may be in the range of 0.1  $\Omega$ /Oersted. The objective in fabricating this sensor device is to measure a typical distance, which is in the order of 1 nm. The sensitivity and response time of the mechanical assembly will depend on the coupling

between the membrane (moving microstructure) and the GMR element. The maximum response time will be in the range of  $10 - 0.2 \mu\text{sec}$  for 1 nm displacement of moving part. A dogbone structure has been used to fabricate GMR element that has a resistance,  $R$  that depends on the local field,  $H$  due to hard magnetic thin film at the GMR sensor. If the resistance is used to measure field intensity the displacement “ $d$ ” may be determined with a simple inversion of the function  $H$  as described in eqn. 4. [8-10]

**Patterning of spin valve or GMR sensor element:** The GMR sensor element may be fabricated using several layers of various metallic thin films patterned by using photolithography. Patterning of GMR element can be achieved by hydrochloric acid plasma, lift-off technique, ion milling, or chemical etching. Patterning of GMR materials by chemical etching may not yield fruitful results since the GMR element consists of multilayers that could form several galvanic couples in the chemical solutions. Different layers can be etched at different rates in the chemical etching solutions due to the galvanic coupling. We have used a single step self-aligned photolithographic lift-off process to achieve the patterning of GMR elements in this study. There may be some technical problems associated with the poor edge definition of GMR elements in the lift-off process. [11]

**Hard magnetic thin film materials:** A hard magnetic thin film element will be deposited over the moving microstructure (membrane) and patterned using an appropriate technique. The lift-off technique may be used to pattern the hard magnetic thin film. Adhesion will be improved by depositing Cr by magnetron sputtering. Co-sputtering of CoCrTaPt will be deposited by lift-off technique. There is no wet etching solution available to pattern CoCrTaPt, FePt, CoPt to act as a hard magnetic thin film.[8] We have used a shadow mask to fabricate a hard magnetic thin film element over the microstructure of silicon nitride.

**Fabrication of moving microstructure:** A moving microstructure of silicon, silicon nitride, or silicon dioxide may be fabricated using various approaches. A silicon membrane may be fabricated using anisotropic etching of silicon using silicon nitride mask and a potassium hydroxide solution. It is very difficult to fabricate a silicon membrane of 1  $\mu\text{m}$  or less using this chemical etching solution approach. A silicon membrane may also be fabricated using a plasma-etching approach. Deep reactive ion etching (DRIE) technique has been used to etch the silicon substrate at a rate of 5 – 10  $\mu\text{m}/\text{min}$ . Aluminum can be used as a mask to fabricate silicon membranes. It has been observed in our study that there will be a micromasking effect with aluminum in the RIE etched area. Thick photoresist has been used as a mask to etch silicon by RIE to fabricate silicon membranes.[12-14] It is difficult to fabricate 1  $\mu\text{m}$  or less thick silicon membranes by RIE since the etching rate is significantly high. Therefore, an alternative approach could be silicon on insulator (SOI) substrate to fabricate silicon membranes. One may etch silicon either by RIE or chemical etching solutions. It is possible to fabricate 3 –5  $\mu\text{m}$  thick silicon membranes. However, we need 1  $\mu\text{m}$  or less thick silicon membranes to use as a moving microstructure to implement in the GMR sensor device. Finally, we have chosen to fabricate a silicon nitride membrane, which is apparently quite stable in hot KOH solution. Silicon nitride has been grown on both sides of a silicon substrate using low-pressure chemical vapor deposition. The  $\text{Si}_3\text{N}_4$  was patterned and then plasma etched down to the silicon substrate. The silicon substrate was etched in hot KOH solution until the other silicon nitride is reached. Thus 0.5  $\mu\text{m}$  silicon nitride membranes are fabricated over silicon substrates.

## Results and Discussion

Figure 3 show scanning electron micrographs of silicon membranes fabricated using photolithography, plasma etching of silicon nitride, and anisotropic etching of silicon. LPCVD silicon nitride has been used as a mask to etch silicon substrate and subsequently to fabricate the silicon nitride membrane. We have successfully fabricated a  $\sim 0.5 \mu\text{m}$  LPCVD silicon nitride membrane to assemble the eventual device as shown in the Fig. 2. Figure 3a and 3d show the backside and front side view of the silicon nitride membrane. Figure 3b shows the cross-section of silicon nitride membrane to evaluate the thickness of the silicon nitride film ( $\sim 0.5 \mu\text{m}$ ). Figure 3c shows the micrograph of the damaged membrane that might indicate the presence of stress in the LPCVD film. We have fabricated silicon nitride membranes of various sizes such as 2 mm x 2 mm to 5 mm x 5 mm.

Figure 4 shows the schematic diagram of the GMR element fabrication. A silicon substrate has been chosen and oxidized by thermal oxidation. The photoresist was spin coated and patterned using photolithography. Tantalum was deposited for electrical contact and to isolate the permalloy from the silicon dioxide. A sensing layer of permalloy was deposited and subsequently cobalt, copper, cobalt, iron-manganese, and finally tantalum were deposited in the same deposition set-up using the same ultra high vacuum chamber. Cobalt was deposited to separate the mixing of permalloy and copper and also the mixing of iron-manganese and copper. Copper is deposited to act as a spacer in this device. The top tantalum layer is deposited to protect the device from oxidation and contamination with other impurities such as carbon and oxygen. [7, 14-17]

Figure 5a shows the scanning electron micrograph of the fabricated GMR element over the silicon dioxide/silicon substrate using lift-off technique. Figure 5b and 5c show the magnified

views of the single GMR element and a corner of the GMR element, respectively. Figure 6(a-f) show the scanning electron micrographs of the GMR element in various regions of the device. The lift-off technique employed in this experiment has yielded poor edge definition. We feel that, this might effect the anticipated reliable sensor response results. Therefore, a technique will be needed to pattern the GMR to yield a perfect vertical sidewall.

During the growth of GMR element stack, a magnetic field is applied to the sample to induce easy and hard axes in the magnetic layers and set the direction for the pinning field in the antiferromagnetic layer. In operation the magnetic field to be sensed is applied parallel to the hard axis since there is very little hysteresis along this direction and the response is linear for small changes in field. Figure 7 is a plot of the resistance change versus the field applied along the hard axis. The change in resistance was about 3.9 % over the entire field range. There are some issues with the lift-off that lead to a less than ideal GMR curve in Fig. 7. Specifically, any surface contamination left after the development of the photoresist will result in rough layers. Rough or wavy interfaces in GMR device increases the ferromagnetic coupling between the two magnetic layers. Also, if the walls of the resist were not perfect additional magnetic coupling could arise.

Figure 8 shows the power versus the frequency when an ac field was applied to the GMR device along with a dc bias field of 15 Oe. The magnitude of the field applied in Fig. 8 was 0.6 Oe (500 Hz sine wave) and the current through the device was 6 mA (device resistance is about 480 K $\Omega$ ). The absence of higher harmonic peaks indicates that there was little distortion and an output of pure sine wave. The baseline noise in Fig. 8 is due to intrinsic 1/f noise in the spin valve. 1/f noise is the dominant noise source until about 20 KHz depending on the current, at higher frequencies thermal noise is dominant. The magnitude of the 1/f noise increases as the square of the current.

Table 2 shows the some of the experimental spin valve configurations that have been fabricated and characterized. Adding the cobalt layer in the GMR device structure has significantly improved the device characteristics. Further experiments are underway to understand the significance of the various layers.

Table 3 shows the test results on the some of the fabricated GMR devices. The change in resistance was high (6.3%) when there is thick cobalt layer and also the permalloy layer was absent. A permalloy layer has been incorporated in the device 2 and cobalt layer thickness layer has been reduced to 15 Å. The change in resistance has reduced to 4.5%. The cobalt layer has been completely eliminated in the device 3 and the change in resistance has been reduced further. The copper layer thickness is different from the critical thickness required to obtain high change in resistance. Further experiments are underway to characterize the various GMR device configurations.

Atomic force microscopy has been used to characterize the surface smoothness of the silicon nitride membrane after dicing whole wafer with silicon nitride membranes. Figure 9a clearly shows the non-uniformity of the silicon nitride membrane. This may be due to the silicon dust that has accumulated over the silicon nitride membrane during the dicing process. Same membrane characterized on its backside using AFM. Figure 9b shows the high uniformity of the silicon nitride membrane. Therefore, it is highly desirable to clean the thin membranes of silicon nitride after dicing. Therefore, a careful experimentation is needed to clean the diced silicon nitride membranes since they are used as a substrate to fabricate hard thin film magnet structure. If the membranes are not cleaned properly there could be serious reliability issues in operating the packaged GMR sensor device. The silicon dust present over the membrane could short the GMR

element and the hard thin film over the microstructure. A process is under development to clean the membrane of dust free silicon.

Figure 10a shows the manually packaged complete GMR sensor device that includes GMR element, silicon nitride microstructure, and a hard thin film magnet deposited over the microstructure. We have used to bond two silicon chips as described in Fig.2 using epoxy. This has yielded a separation of GMR element and hard thin film magnet of more than few microns, which might have resulted in due to the epoxy and possibly due to the silicon dust particles. Such large separation could result in an insignificant effect of magnetic field due to the hard thin film magnet over the GMR element to effect its resistance characteristics. Therefore, alternative approaches are needed to assemble the two chips to study the GMR characteristics as a function of distance and various hard magnetic materials deposited over the microstructures. We will report these results in the future publications.

## CONCLUSIONS

We have used the appropriate layers such as sensing layer, conducting spacer and antiferromagnetic layer and other layers to avoid the mixing of the sensing layer and conducting spacer. Identified the problems associated with the fabrication of very thin silicon membranes and we have fabricated 0.5 micron low pressure chemical vapor deposited silicon nitride membranes using anisotropic chemical etching of silicon and plasma etching of silicon nitride. Identified the hard magnetic thin film, which will be deposited over the moving silicon nitride microstructure to demonstrate the GMR sensor device. We have manually assembled for the first time the GMR element, hard magnetic thin film fabricated over moving silicon nitride microstructure components to fabricate GMR/MEMS sensor device. There are some practical problems associated with

bonding of the two silicon chips appropriately. Individual GMR element has shown a change of resistance 3.9% as a function of magnetic field. We have studied the change in resistance as a function of spin valve configuration. Without the cobalt layer the GMR response has decreased shows the significance of Co in the GMR element stack. The presence of cobalt and permalloy will significantly effect the GMR response results of the device. We will be reporting the results further on this type of GMR sensor devices in our future publications.

### **ACKNOWLEDGMENTS**

This research work was carried out at the Jet Propulsion Laboratory, California Institute of Technology and Rice University and was supported by NASA through Langley Research Center.

## REFERENCES

1. M. N. Baibich, J.M. Broto, A. Fert, F. Nguyen Van Dau, F. Petroff, P. Etienne, G. Creuzet, A. Friederich, and J. Chazelas, *Phys. Rev. Lett.* 61 (1988) 2472.
2. S.P. Parkin, "Giant Magnetoresistance in sputtered magnetic superlattices", 35<sup>th</sup> Annual conference on magnetism and magnetic materials, November 27 – December 4, 1989. Abstract was published in *Journal of Applied Physics*, 67, 5931 (1990).
3. Nonvolatile Electronics Inc., *Engineering & Application Notes*, <http://www.nve.com>.
4. P. Grunberg, "Magnetic field sensor with ferromagnetic thin film layers having magnetically antiparallel polarized components," U.S. Patent 4,949,039.
5. B. A. Gurney, V.S. Speriosu, D.R. Wilhoit, H. Lefakis, R.E. Fontana, Jr., *J. Appl. Phys.*, 81 (1997) 3998.
6. R.J. M. van de Veerdonk, P.J. Belein, K.M. Schep, J.C.S. Kools, M.C. de Nooijer, M.A. Gijs, R. Coehoorn, W.J.M. de Jonge, *J. Appl. Phys.*, 82 (1997) 6152.
7. W.F. Egelhoff, Jr., P.J. Chen, C.J. Powell, M.D. Stiles, R.D. McMichael, C.L. Lin, J.M. Sivertsen, J.H. Judy, K. Takano, A.E. Berkowitz, T.C. Anthony, and J.A. Brug, *J. Appl. Phys.*, 79 (1996) 5277.
8. S. Mao, N. Amin, and E. Murdock, *J. Appl. Phys.*, 83 (1997) 6807.
9. A. Wallash, *Data Storage, Test and Measurement*, January 1998, p. 37.
10. J. Szucs, T. O'Brien, and D.K. Lottis, S. Gangopadhyay, S. Mao, and E. Murdock, *J. Appl. Phys.*, 81 (1997) 4014.
11. M. Xiao and M.H. Kryder, *Electrochemical Society Proceedings, Proceedings of the Fourth International Symposium on Magnetic Materials, processes and Devices, Application to*

- storage and microelectromechanical systems (MEMS), Edited by L.T. Romankiw and D. A. Herman, Jr., Vol. 95-18, p. 51 (1995).
12. C. D. Ellis, Aburn University, Personal communication, January 1998.
  13. R. Ramesham, C.D. Ellis, J.D. Olivas, and S. Bolin, *Thin Solid Films*, 330 (1998) 62.
  14. Marc Madou, *Fundamentals of Microfabrication*, CRC Press, New York, 1997.
  15. V.S. Speriosu, J.P. Nozieres, B.A. Gurney, B. Dieny, T.C. Huang, and H. Lefakis, *Physical Review B*, 47 (1993) 11579.
  16. J.P. Nozieres, V.S. Speriosu, B.A. Gureny, B. Dieny, H. Lefakis, and T.C. Huang, *J. Magnetism and Magnetic Materials*, 121 (1993) 386.
  17. B. Dieny, *J. Magnetism and Magnetic Materials*, 136 (1994) 335.

## FIGURE CAPTIONS

1. Energy dispersive x-ray analysis of stacked GMR sensing element.
2. Schematic diagram of complete giant magnetoresistive (GMR) sensor device fabrication.
3. Scanning electron micrographs (a-d) of silicon nitride membranes fabricated using anisotropic etching of silicon substrate.
4. Schematic diagram of multilayer GMR element used in GMR/MEMS sensor device.
5. SEM of fabricated GMR device (a) complete chip with several GMR elements, (b) single GMR element, and (c) magnified view of GMR element.
6. Scanning electron micrographs (a-f) of the fabricated GMR device to identify the edge definition of GMR element.
7. Resistance change in the GMR sensor device vs. the applied magnetic field.
8. Power vs. the frequency used to test the GMR sensor device.
9. Surface smoothness characterization of silicon nitride membranes by using atomic force microscopy (AFM). (a) Topside of the membrane and (b) backside of the membrane.
10. Scanning electron micrographs of the (a) manually assembled GMR/MEMS sensor device and (b) magnified view of the GMR sensor element and hard magnetic thin film over microstructure.

**Table 1: Sputter Deposition of the Multilayers in UHV Chamber to fabricate GMR Element**

Base pressure	$1 \times 10^{-8}$ Torr
Substrate	Thermally grown SiO <sub>2</sub> /Si
Pressure	1 mTorr
Temperature	20±5°C
Substrate-target separation	6 inches (15.2 cm)
Sputtering power	40 W (Ta) 50 W (Co and Permalloy) 30 W (FeMn, Cu)
Deposition rate	1 Å/sec

**Table 2: The change in resistance as a function of spin valve configuration [16]**

Device #	Spin Valve Configuration	$\Delta R/R$	Oe
1	Co/Cu/Co/FeMn	9.9%	0.81
2	NiFe/Cu/NiFe/FeMn	4.3%	1.51
3	NiFe/Co/Cu/Co/NiFe/FeMn	9.1%	--

**Table 3: GMR Device Test Results**

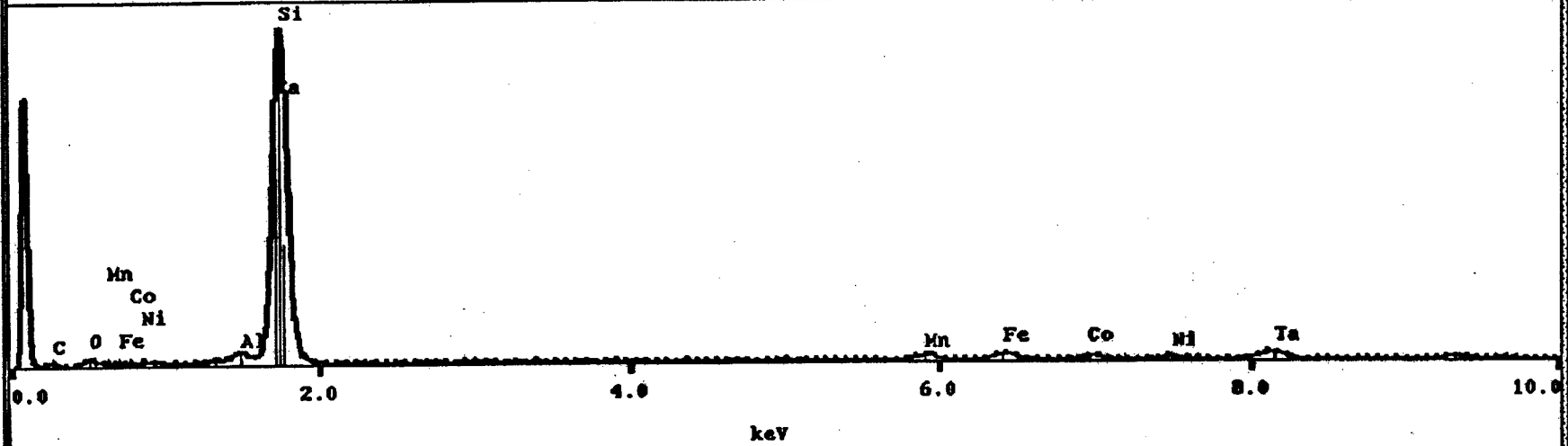
Device #	Ta (Å)	Py (Å)	Co (Å)	Cu (Å)	Co (Å)	Py (Å)	FeMn (Å)	Ta (Å)	$\Delta R/R$
1	64	--	50	44	50	--	80	64	6.3%
2	50	50	15	44	15	50	80	50	4.5%
3	50	50	--	44	--	50	80	50	1.6%

X-ray Display 1

Acquisition completed.

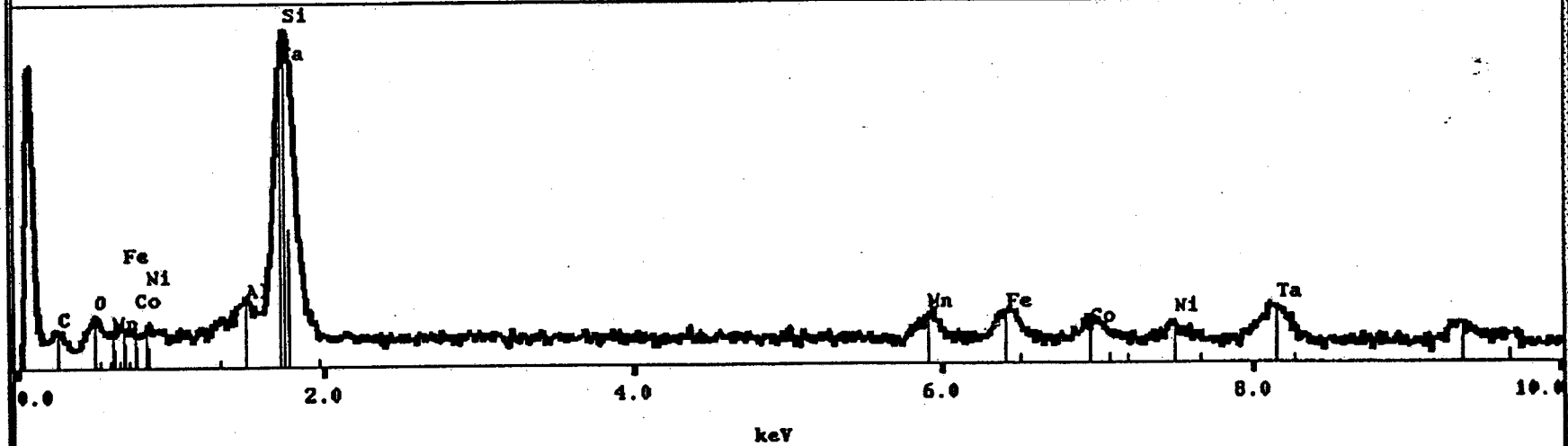
✓ Window 1  
— ✓ sample

2076 FS



Window 2  
— ✓ computed\_display 100. \* Sqrt #1:2:1

4556 FS



R\_GMR09

Figure 1: Ramesham et al.,

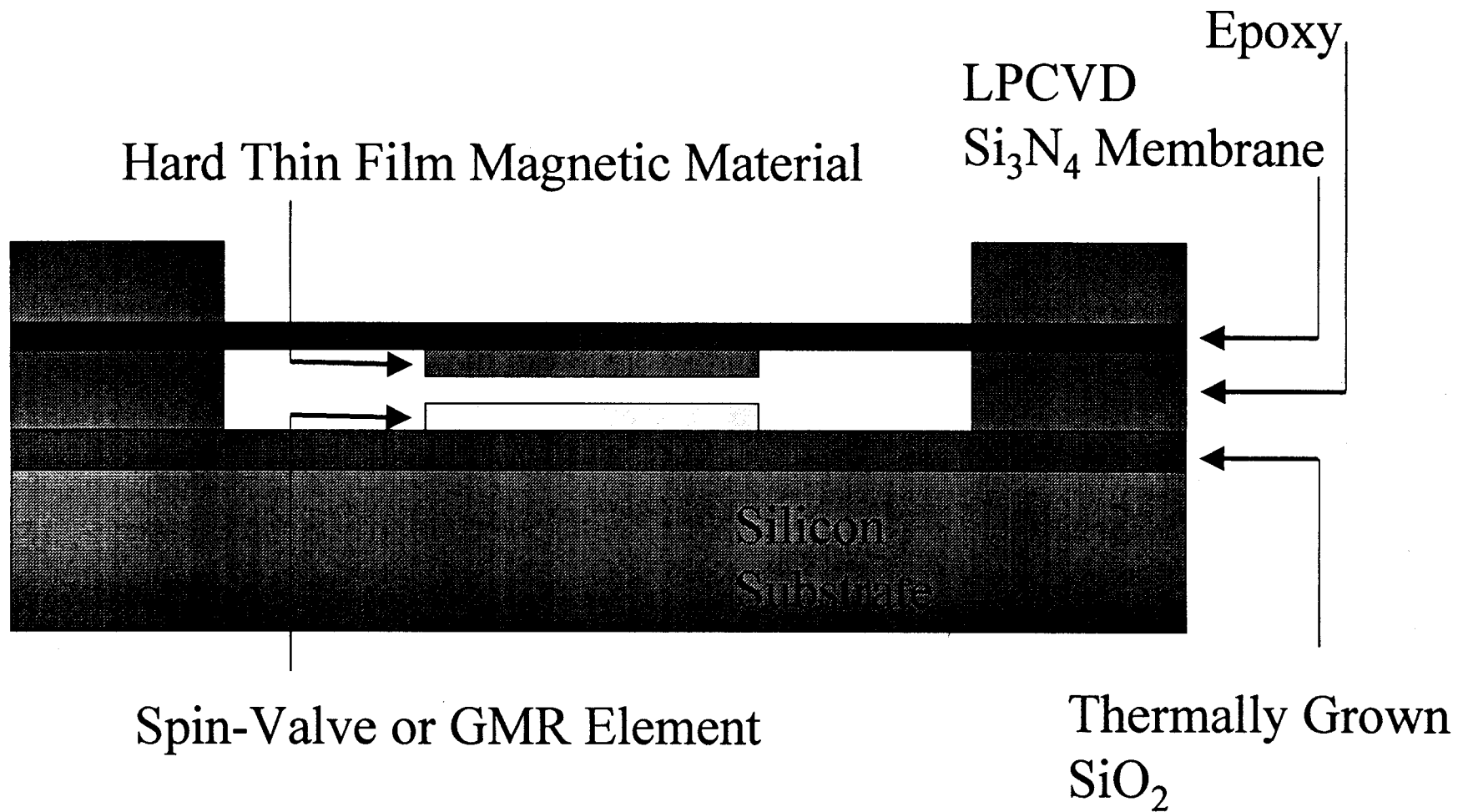


Figure 2: Ramesham et al.,

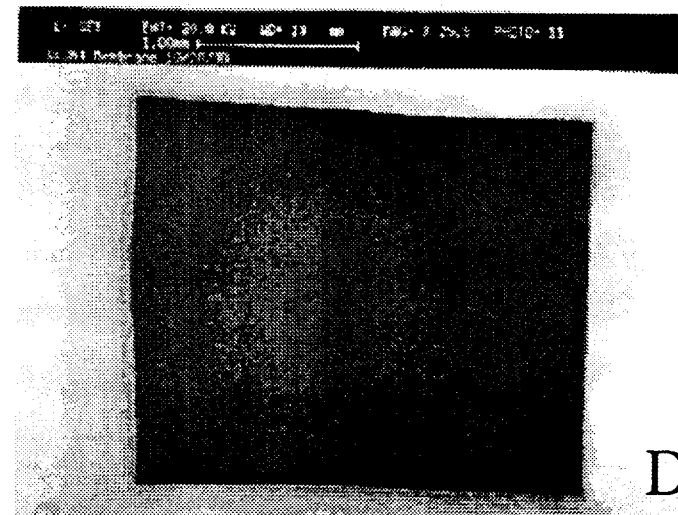
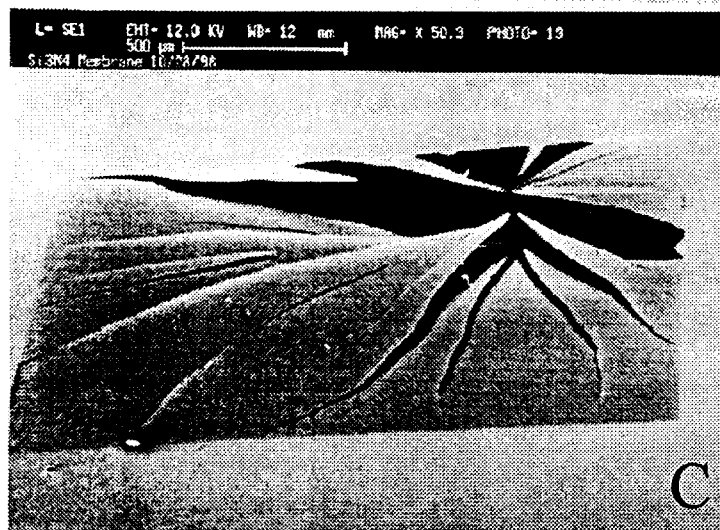
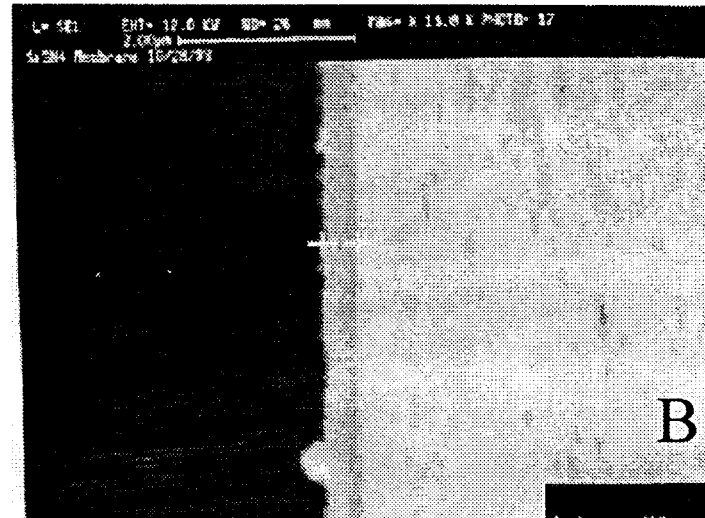
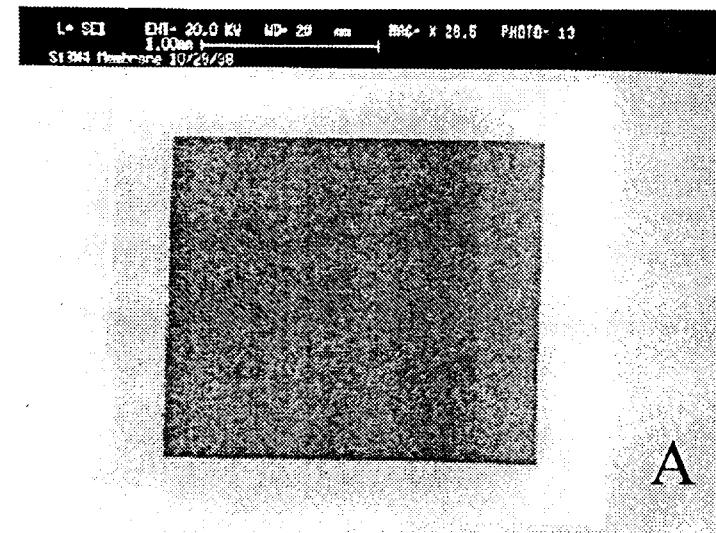


Figure 3: Ramesham et al.,

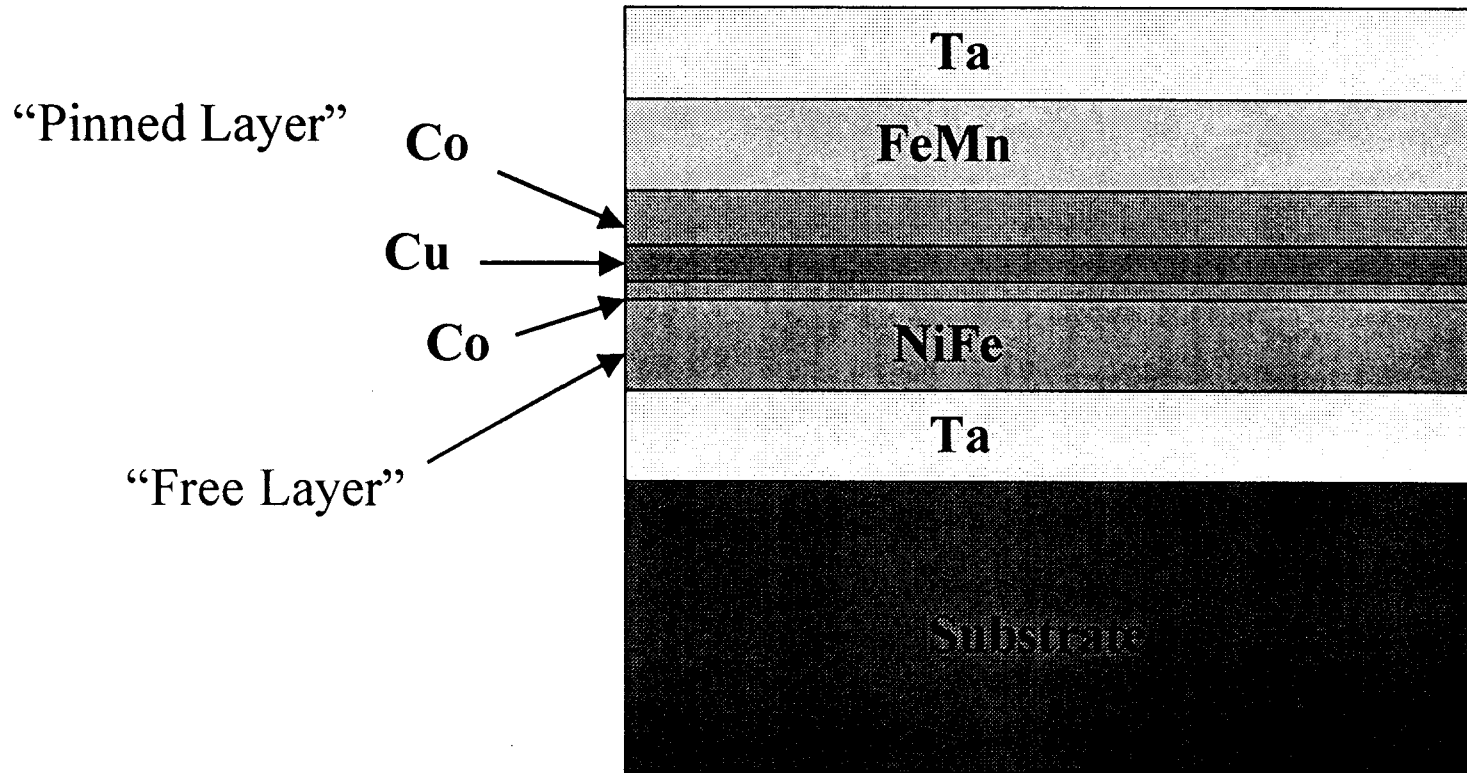


Figure 4: Ramesham et al.,

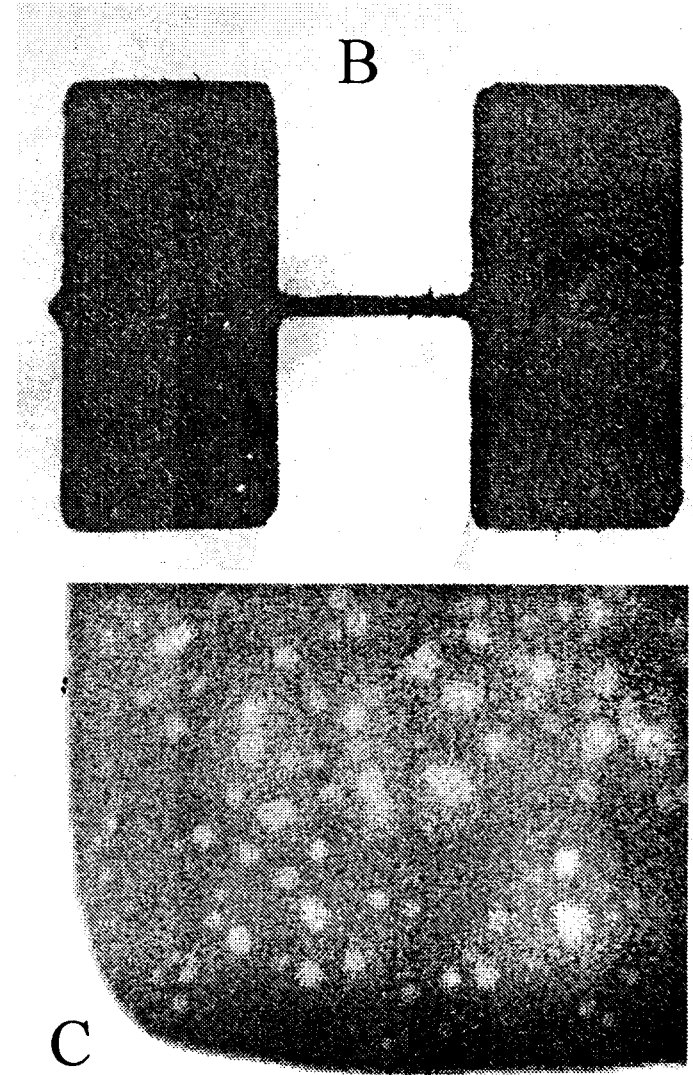
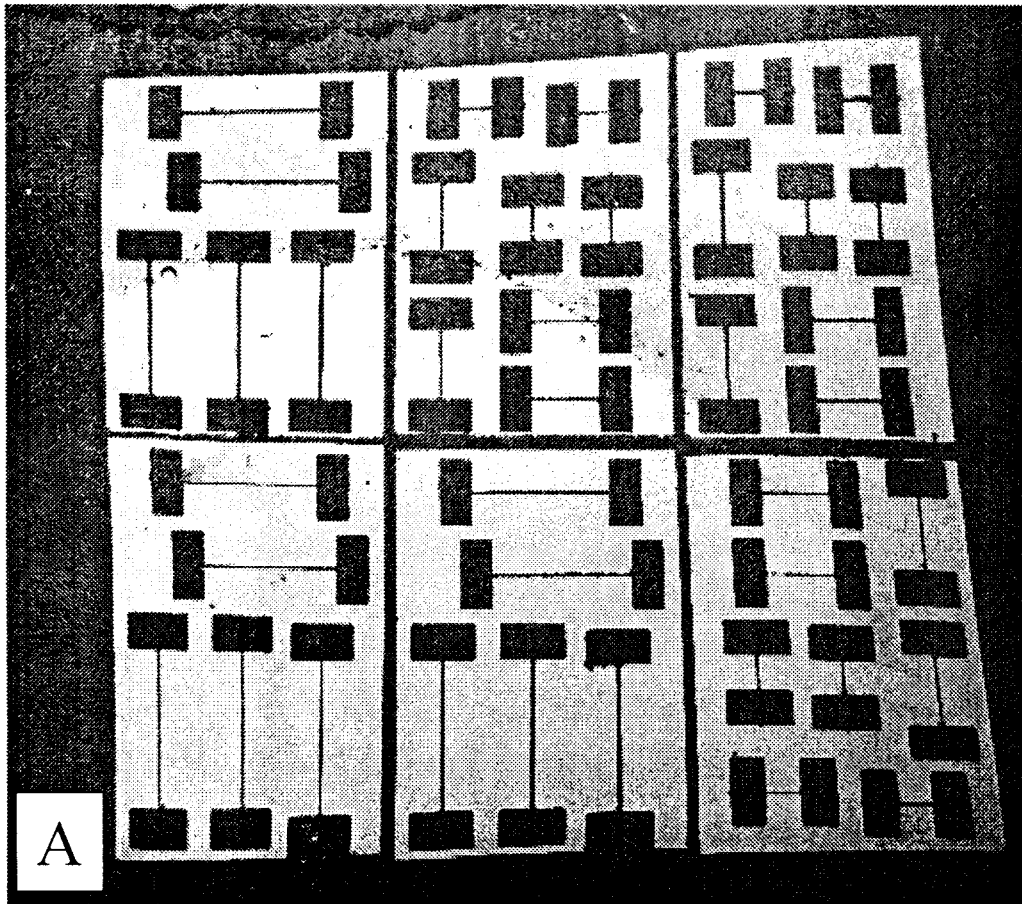
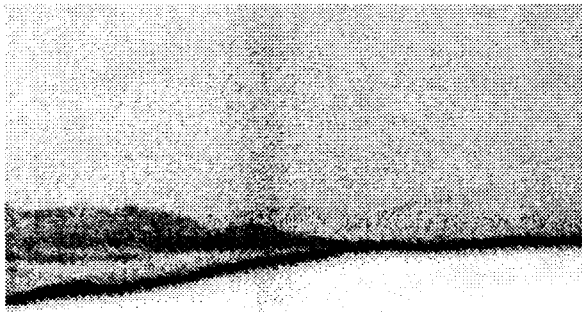
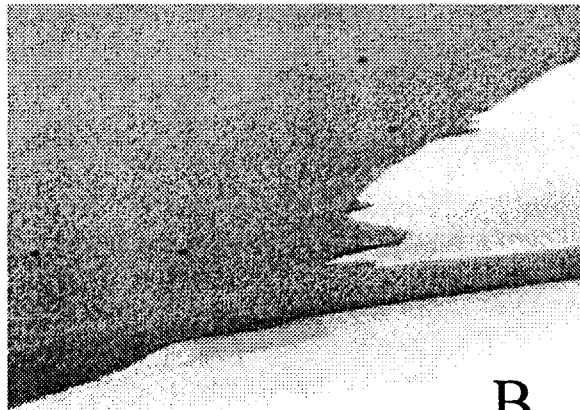


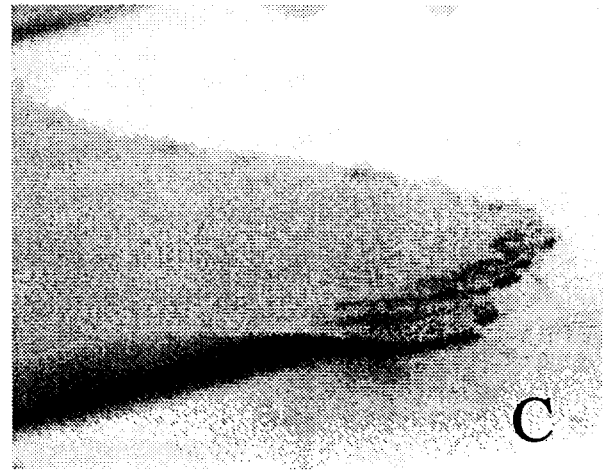
Figure 5: Ramesham et al.,



A



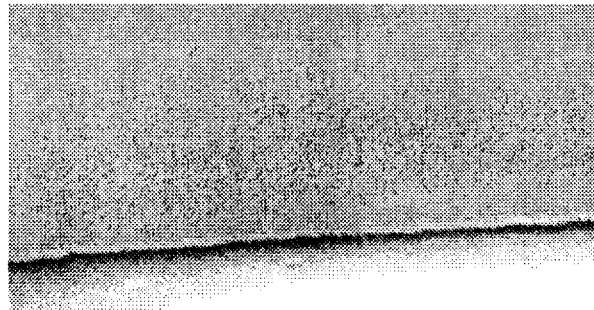
B



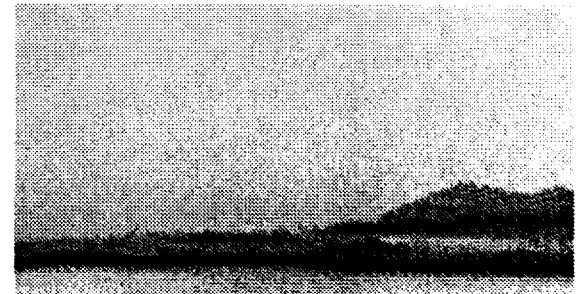
C



D



E



F

Figure 6: Ramesham et al.,

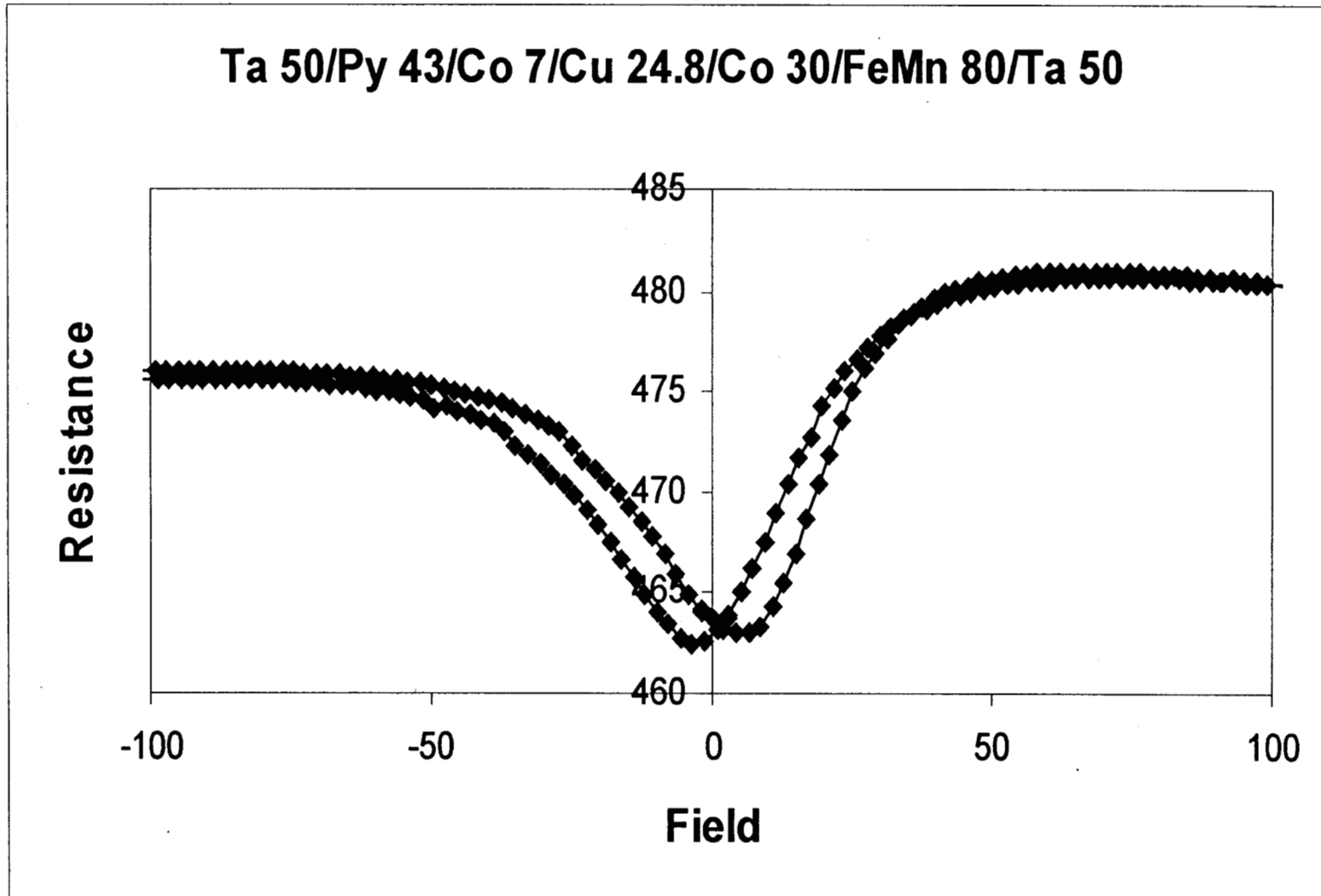


Figure 7: Ramesham et al.,

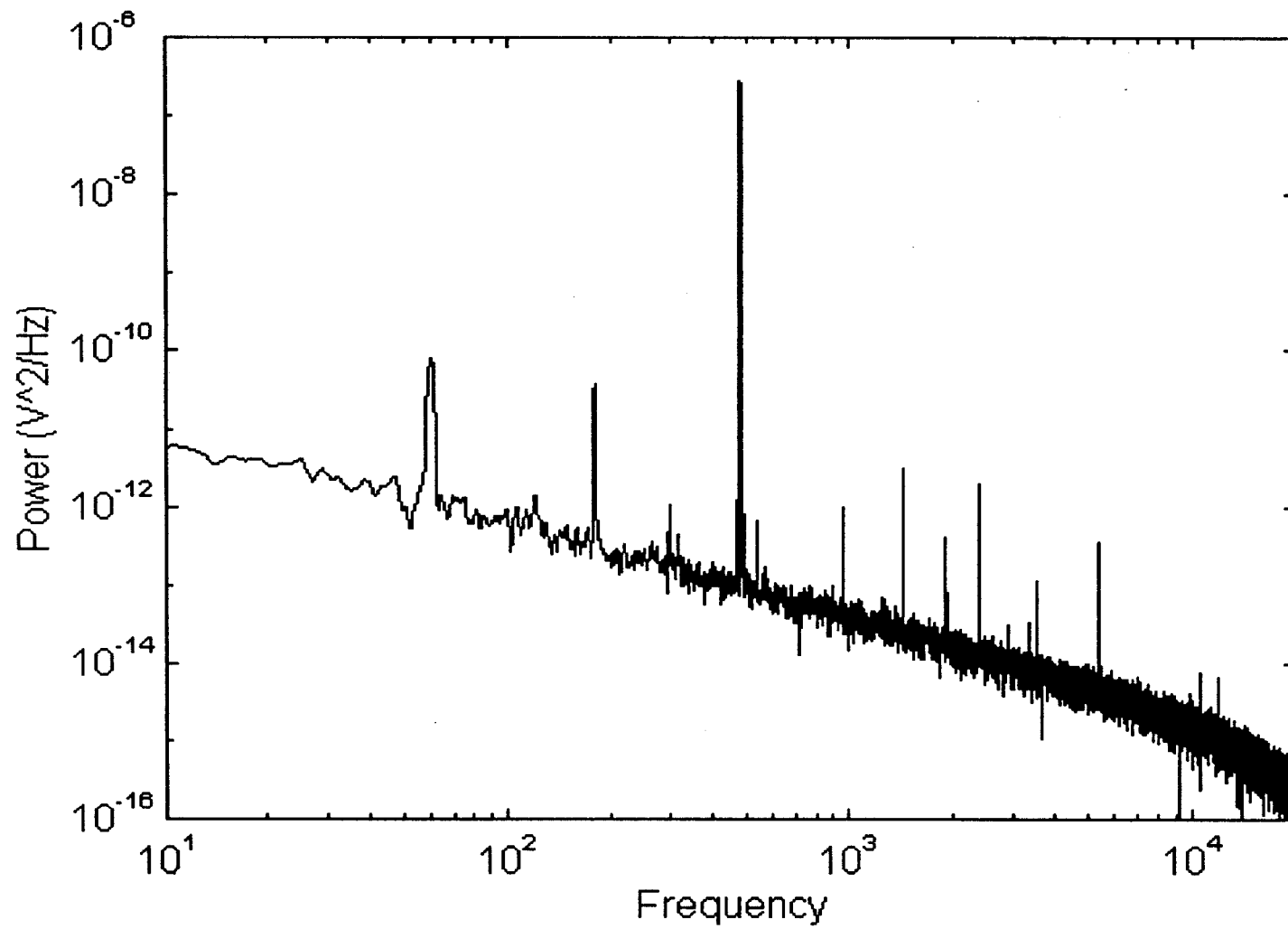
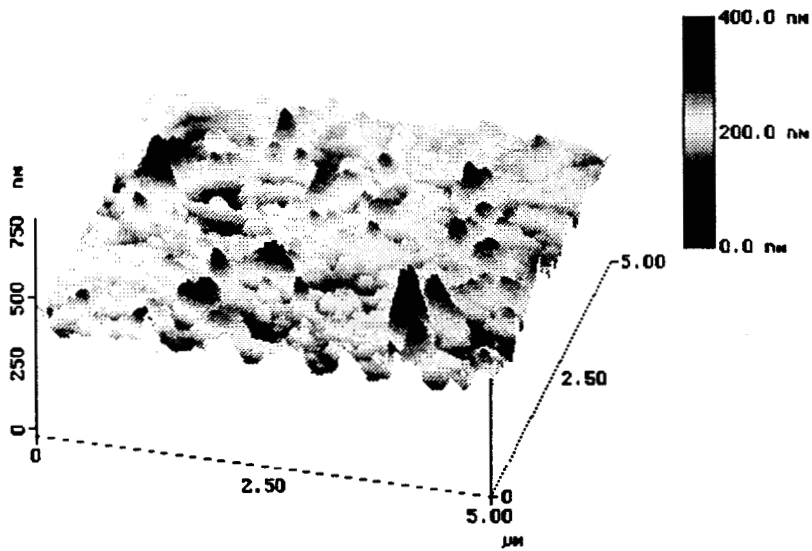
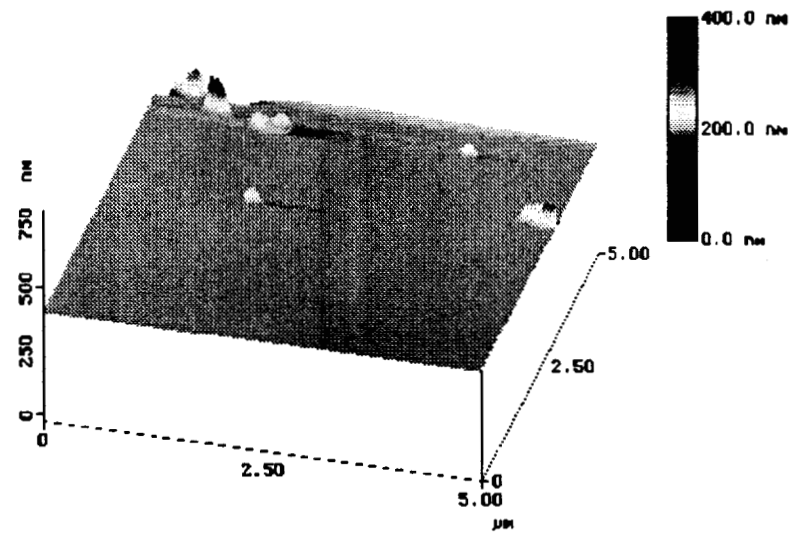


Figure 8: Ramesham et al.,



Membrane Front, RMS=34.5nm



Membrane Back, RMS=5.17nm

Figure 9: Ramesham et al.,

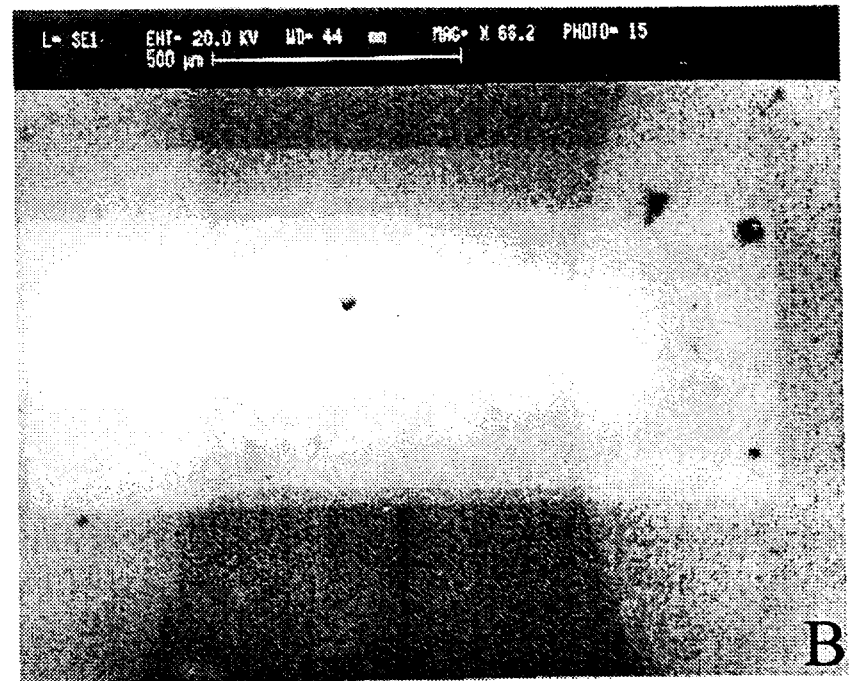
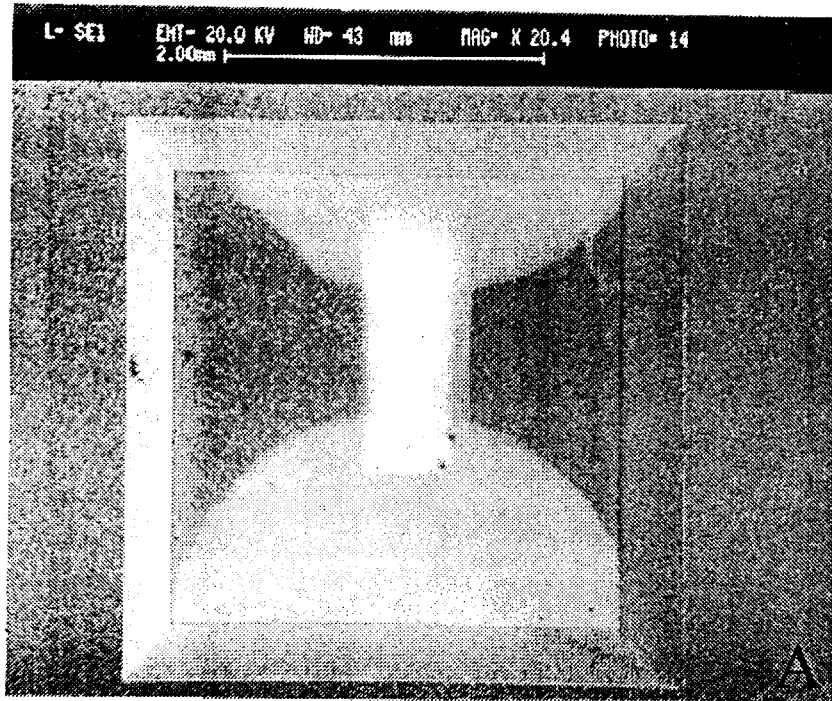


Figure 10:Ramesham et al.,